Liquefaction Centrifuge Modeling in Non-homogeneous Soil Deposits

M. Maharjan & A. Takahashi
Tokyo Institute of Technology, Tokyo, Japan

SUMMARY:
A series of centrifuge model tests were conducted on uniform, layered, and non-homogenous soil deposits. The non-homogeneous soil consisted of discontinuous soils of different permeability, arranged horizontally in sand. The layered soil consisted of uniform sand overlain by a continuous layer of relatively impermeable soil. Effects of discontinuous layers on the behavior of liquefiable sand layers are examined. The test results show that during liquefaction silt layer prevents the upward movement of pore water and the pore water finds a path to drain from high pore pressure region to low pressure region. More excess pore water pressure was accumulated for a longer period of time after shaking in a non-homogeneous soil deposit than in a homogeneous soil, resulting in uneven settlements of soil surface.

Keywords: Liquefaction, non-homogeneous, centrifuge model test, excess pore water pressure

1. INTRODUCTION

Liquefaction, which involves substantial loss of strength and stiffness of saturated sandy soils due to seismic loading, is one of the most dramatic threats to the safety of structures during earthquakes. The generation of pore pressure plays a key role in all liquefaction-related phenomena (Kramer 1996). When this pore pressure reaches a value equal to the total overburden stress, soil particles do not support each other, referred as a zero effective stress condition; a state of initial liquefaction (National Research Council 1985, Fiegel and Kutter 1994, Brennan and Madabhushi 2005).

While most of the earlier physical model tests on liquefaction problems have dealt with uniform clean sand, more recent studies have employed horizontally layered soil (with uniform properties within distinct soil layers). Fiegel and Kutter(1994) conducted several centrifuge model tests on layered soil and concluded that the presence of relatively impermeable layer (silt) within the liquefiable deposits results in the formation of a water film beneath it. Kokusho and co-workers conducted several model tests and found that excess pore water squeezed from the liquefied sand is trapped by a relatively impermeable sub-layer and forms a water film beneath it, which has a key role in the extent of lateral deformations in the sloping surface (Kokusho 1999, Kokusho 2000, Kokusho and Kojima 2002). Kulasingam et al.(2004) conducted several centrifuge tests with and without silt interlayer to demonstrate the potential of void redistribution to cause strain localizations and associated deformations. However, real soil profile is complex and the soil layer is never uniform or continuous even in case of layered soil. Ghosh et al.(2005) performed a series of centrifuge tests to analyze the effects of localized loose sand in a dense sand deposit subjected to seismic loading. It was found that the soft layer has significant influence on the overall response of the layered strata. Chakrabortty and Popescu(2012) also conducted a series of centrifuge tests on homogeneous and heterogeneous soil deposits followed by numerical simulation, where the heterogeneous model consisted loose pockets of same sand with lower relative density. The results showed more excess pore water pressure is generated in a heterogeneous soil deposits than in corresponding homogeneous soil. However, the stratification of soil profile is not only limited to soft layers involving one type of soil material; it

consists of many discontinuous layers ranging from highly permeable liquefiable to impermeable non-liquefiable layers. To the best knowledge of authors, numerical or experimental studies related to the presence of discontinuous less permeable layer in the liquefiable soil have not been carried out. Therefore, liquefaction potential of non-homogeneous soil profile is not well understood, though many liquefaction case histories exist.

This paper presents the results of three dynamic centrifuge tests on saturated uniform, layered, and non-homogeneous soil profile specimens. Non-homogeneity was incorporated by including periodically distributed silt patches with a lower permeability than the liquefiable soil specimen with the same length of discontinuities in each layer which will be referred as drainage layer hereafter. Laminar containers were used in all the tests to properly simulate the boundary conditions. The primary purposes of this series of tests is to systematically study the effects of non-homogeneity of the soil deposit on the amount of excess pore water pressure, drainage path and settlement of the liquefiable soils.

2. TESTING PROGRAM AND MODEL DETAILS

Three centrifuge model tests were performed on the Tokyo Tech Mark III centrifuge (Takemura et al. 1999) at a centrifugal acceleration of 40g. The model configurations and the entire test results are presented and discussed in prototype scale units, unless indicated otherwise.

Table 1 and Fig. 1 depict the model configurations. Three different model geometries were used: Model 1 is a homogeneous sand profile (Fig. 1(a)); Model 2 consists of sand layer overlain by continuous silt layers (Fig. 1(b)); Model 3 consists of sand layer overlain by discontinuous silt layers with the same length of drainage layer (Fig. 1(c)). Toyoura sand and Silica sand No.8 were used for the tests (Table 2). The thickness of silt layer in all models was 1.0 m, while the soil thickness was 9.8 m with the water table 0.8 m below the surface. The total length of drainage layer in each layer in Model 3 was 5.0 m.

Models were constructed in flexible laminar container with inner dimensions of 50×20×45 cm in length, width and height respectively, which allows the container to deform dynamically with the soil layer. The models were prepared by air pluviation method, where sand was poured from a hopper which was moved manually forth and back along the longest dimension of the container, and the falling height was kept constant to obtain the desired relative density. The colored noodles 'somen' were placed at the sand-silt interface to trace the deformation pattern. A solution of 1.98% Metolose in water was used to produce a pore fluid having a viscosity 40 times greater than water. The density and surface tension of this solution is practically identical to that of water. It has also been shown in previous research that this type of viscous fluid neither disturbs nor adversely affects the dynamic properties of cohesionless soil (Stewart et al. 1998, Okamura et al. 2001). Therefore, the highly viscous metolose solution ensured accurate simulation of prototype soil permeability of a fine sand and silt when tested at 40g. The de-aired metolose solution was dripped slowly from the top of the container under a vacuum of 760 mmHg until the solution level reached the desired elevation. The

Table 1. Model details

Model code	Model series	Model details	Model height (m)	Depth of water table (m)
Model 1	Uniform sand	D_{r1}=50%	9.8	0.8
Model 2	Continuous silt interlayered sand	D_{r1}=50% D_{r2}=50%, H_{silt}=1m No drainage path	9.8	0.8
Model 3	Discontinuous silt interlayered sand	D_{r1}=50% D_{r2}=50%, H_{silt}=1m Drainage length=5 m	9.8	0.8

Note: D_{r1} and D_{r2} represent the relative density of Toyoura sand and silt respectively. H_{silt} represents the thickness of silt in interlayered sand.

saturation process requires approximately 30 hours. After saturation, the sand was again pluviated to make the total height equal to 24.5 cm in model scale so that the water table was 0.8 m below the surface.

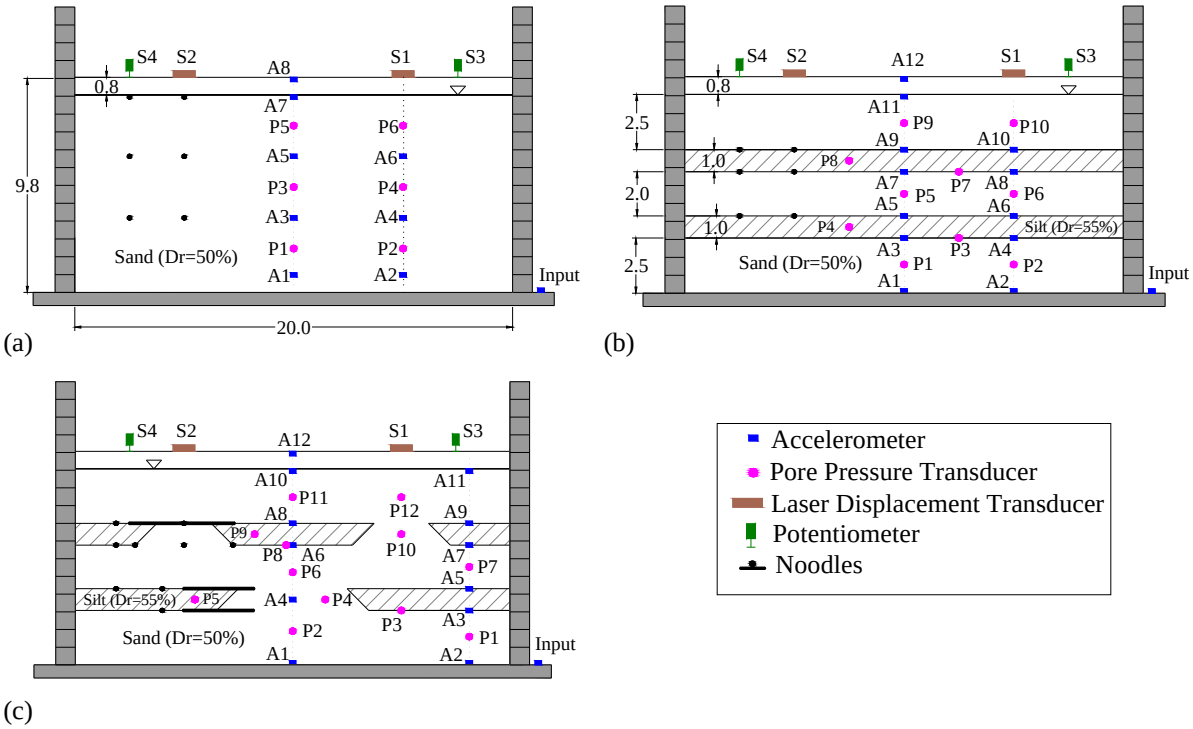

Figure 1. General Model configurations: (a) Model 1; (b) Model 2; and (c) Model 3

Table 2. Index properties of soils

Property	Toyoura Sand	Silica No. 8
Specific gravity, G_s	2.65	2.65
D_{50}	0.19 mm	0.10 mm
D_{10}	0.14 mm	0.041 mm
Maximum void ratio, e_{max}	0.973	1.333
Minimum void ratio, e_{min}	0.609	0.703
Permeability at Dr=50%	2.1×10^{-4} m/s	2×10^{-5} m/s

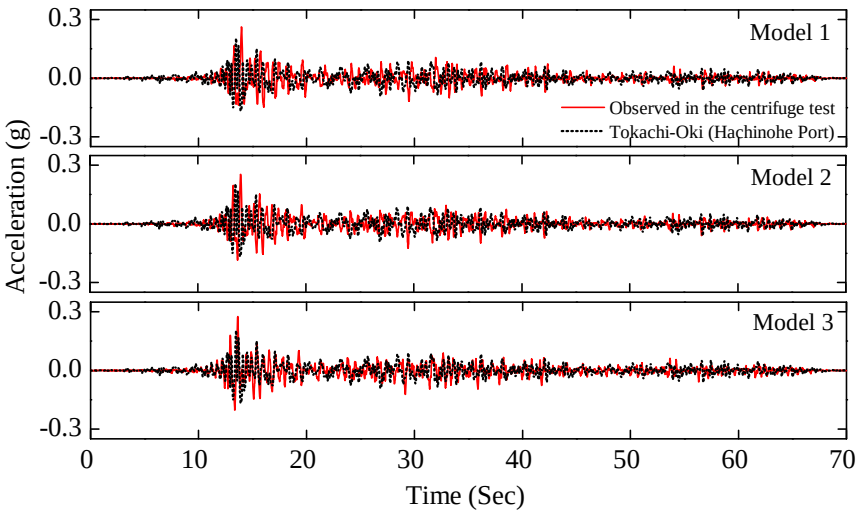

Figure 2. Acceleration time histories of input motion for all the tests

After preparation, the models were placed in centrifuge and spun at centrifugal acceleration of 40g. Earthquake ground motion recorded at the Hachinohe Port in 1968 Tokachi-Oki Earthquake (NS component) was applied at the base of the model parallel to the long sides of the container (Fig. 2). The ground motion applied to the shaker is plotted with a dotted line, and the input motions recorded at the base of the laminar container for each tests are plotted with a solid line. During the experiments, the accelerations were recorded by accelerometer and pore water pressures generated during dynamic loading were measured by pore pressure transducers (PPTs) installed at different locations. The surface settlements were measured by laser displacement transducers and potentiometers. The results were then utilized to assess the soil response mechanism during liquefaction in non-homogeneous soil deposits. The results were analyzed to reveal the differences in the dynamic responses in uniform and non-homogeneous soil deposits.

3. CENTRIFUGE MODEL TEST RESULTS AND DISCUSSIONS

The results of centrifuge model tests will be discussed below in terms of excess pore water pressure, acceleration, and settlement responses.

3.1. Excess pore water pressure responses

Records of pore pressure transducers for three centrifuge model tests are presented in Fig. 3. Changes of excess pore water pressure isochrones for all the model tests are shown in Figs. 4-6. The records of all the PPTs are not shown here for brevity. The locations of transducers were measured before and after each test. The excess pore water pressure, when reaches a value equal to the initial effective stress, indicates the occurrence of liquefaction; a state of initial liquefaction. In most cases the excess pore water pressure tends to exceed the initial effective stress. This might be due to the settlement of the pore pressure transducer or rise in water table (Fiegel and Kutter 1994). The results of the three tests show that excess pore water pressure generation is almost similar in all the tests, while the dissipation is completely different.

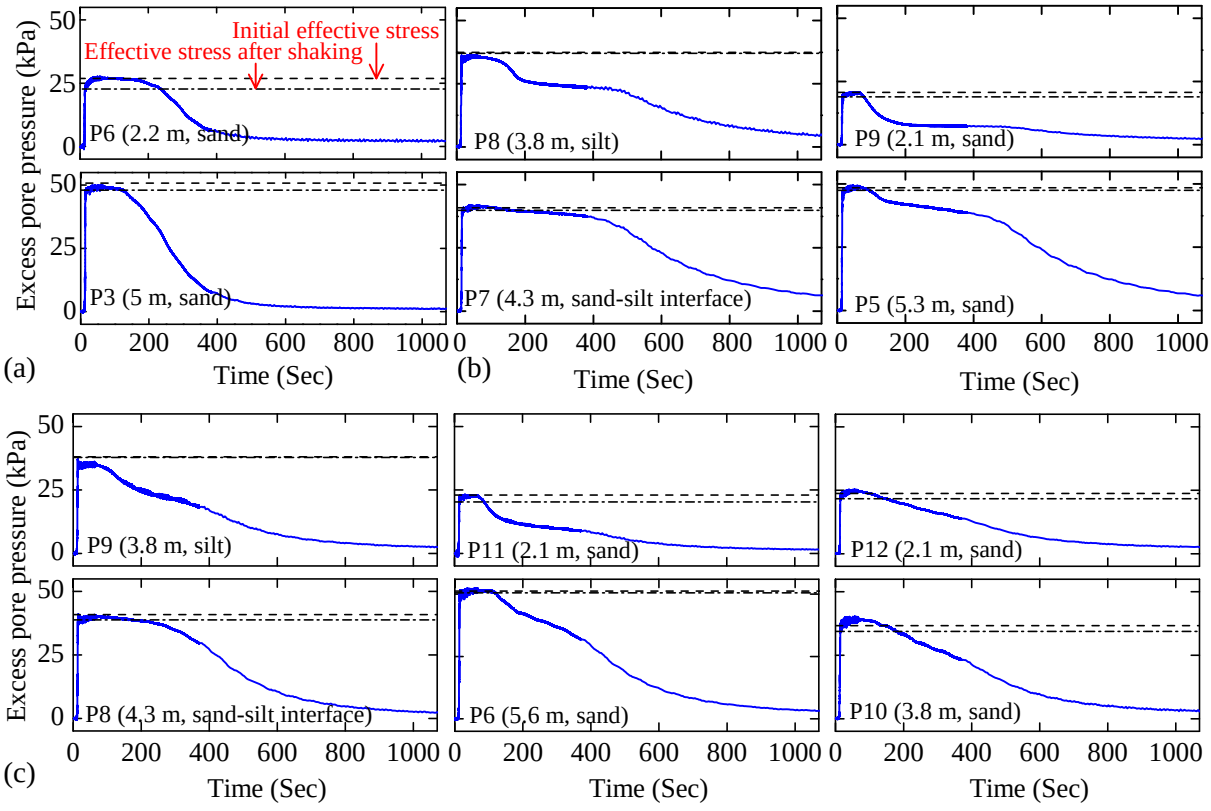

Figure 3. Excess pore water pressure time histories: (a) Model 1; (b) Model 2; and (c) Model 3

In model 1, liquefaction occurred at all the locations of the pore pressure transducers, (Fig. 4(a)), where the excess pore water pressure reached the value equal to the initial effective stress. All of the pore pressure transducers show a rapid rise of excess pore water pressure, reaching liquefaction between 12 s to 15 s of shaking, followed by a rapid dissipation of excess pore water pressure. The elapsed time for complete dissipation of excess pore water pressure is about 400 s (Fig. 4(b)). In model 2 and 3, excess pore water pressures rise rapidly in sand as well as silt (Figs. 5 and 6). However, the elapsed time for dissipation is quite different. The excess pore water pressure rise in silt is caused partly by pore water pressure generated in silt and partly by pore water pressure transmitted from the sand. The excess pore water pressures beneath the upper silt layer remain equal to the initial effective stress for a longer time even after the cessation of dynamic motion, indicating the trapping of pore water. In model 2, it can be seen that the excess pore water pressures measured below the silt have nearly the same rate of dissipation after a certain time, which is about 400 s (P5 and P7, Figs. 3(b) and 5(b)). The faster dissipation of excess pore water pressures after 400 s might be due to rupture of silt layer. The silt layer forms a vent in the form of crack and dissipation of pore pressures is accelerated through sand boils. However, the dissipation of excess pore water pressures above the silt proceeds faster than in model 1 (Figs. 4(b), 5(b), and 6(b)).

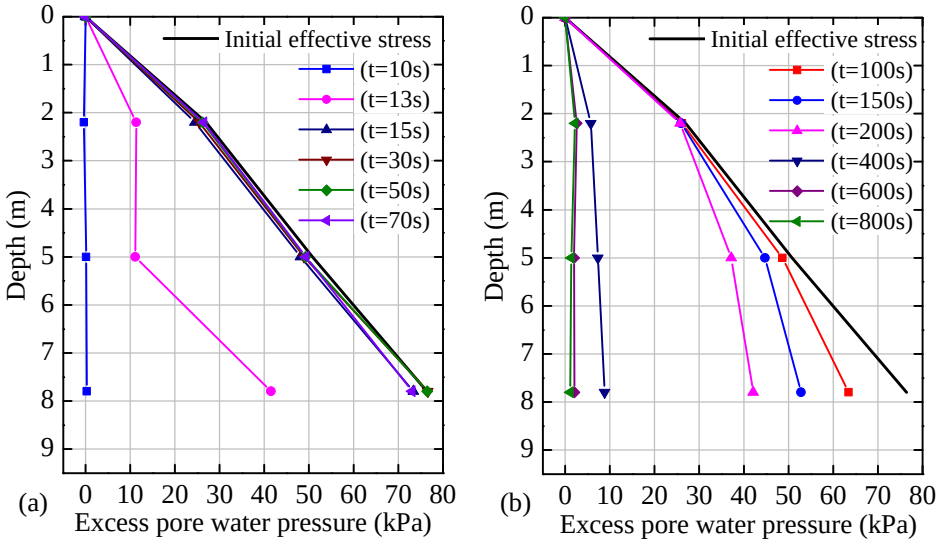

Figure 4. Excess pore water pressure isochrones measured on centerline in Model 1: (a) during shaking; and (b) after shaking

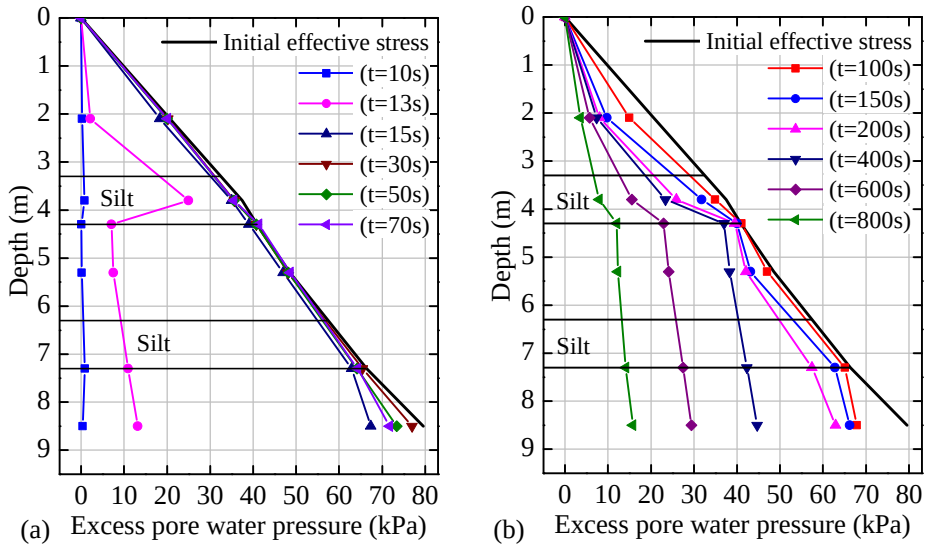

Figure 5. Excess pore water pressure isochrones measured on centerline in Model 2: (a) during shaking; and (b) after shaking

In model 3, it can be seen that the excess pore water pressures measured below the silt have nearly the same rate of dissipation after a certain time, which is about 200 s (P6 and P8, Figs. 3 (c) and 6(b)). The rate of dissipation is comparatively faster than in model 2. This might be due to the presence of discontinuities in silt layer. The silt layer being relatively impermeable does not allow the upward flow of pore water pressures. Had the silt layer been continuous, the pore water would be trapped beneath. During dissipation of pore pressure, the pore pressures at high pore pressure region could easily find a path and could transmit to the low pore pressure region through that path. This causes the dissipation of excess pore water pressure at P10 and P12, which lies in the discontinuity in the slit layer at 3.8 m depth and above the discontinuity at 2.1 m depth respectively, quite different from other pore pressure responses. A comparison can be made between P11 and P12, which are at the same depth but the former is above the silt layer and latter is above the discontinuity in silt layer, i.e. drainage path (Figs. 6(b) and 6(c)). The generation of excess pore water pressures is fairly significant but the dissipation of excess pore water pressures is quite different. The excess pore water pressure remains equal to initial effective stress up to about 200 s at P12, while the excess pore water pressure at P11 dissipates as soon as the shaking stops (Figs.6(b) and 6(c)). This can also be demonstrated by comparing the time histories of excess pore water pressure ratio (r_u) measured at 2.1 m depth for Model 2 and 3 (Fig. 7). As seen, the rate of excess pore water pressure ratio build-up is significantly the same in both pore pressure transducers. On the contrary, the dissipation of excess pore water pressure proceeds slower in P12. The excess pore water pressure reduces to half of the initial value (i.e. $r_u = 0.5$) by the first 150 s at P9 and P10 (Model 2) and P11 (Model 3), but $r_u = 0.9$ at 150 s at P12 (Model 3). The generation of excess pore water pressure in sand is mainly due to the cyclic shearing. However, the difference in dissipation might be due to seepage flow or migration of pore water pressure from high pore pressure region to low pore pressure region. This lateral migration of pore water pressure may be quite substantial in the actual in situ cases where the permeability in lateral direction may be greater than that in the vertical direction. Moreover, the presence of relatively impermeable layer prevents the vertical drainage of pore water pressure during dissipation. The pore water pressure finds a path in lateral direction, from where it can be drained out through the discontinuous part, i.e. drainage path. Figure 7 clearly demonstrates this mechanism; therefore there is a continuous transmission of pore water pressure at P12. This continuous supply of pore water pressures might keep the liquefied condition for long duration.

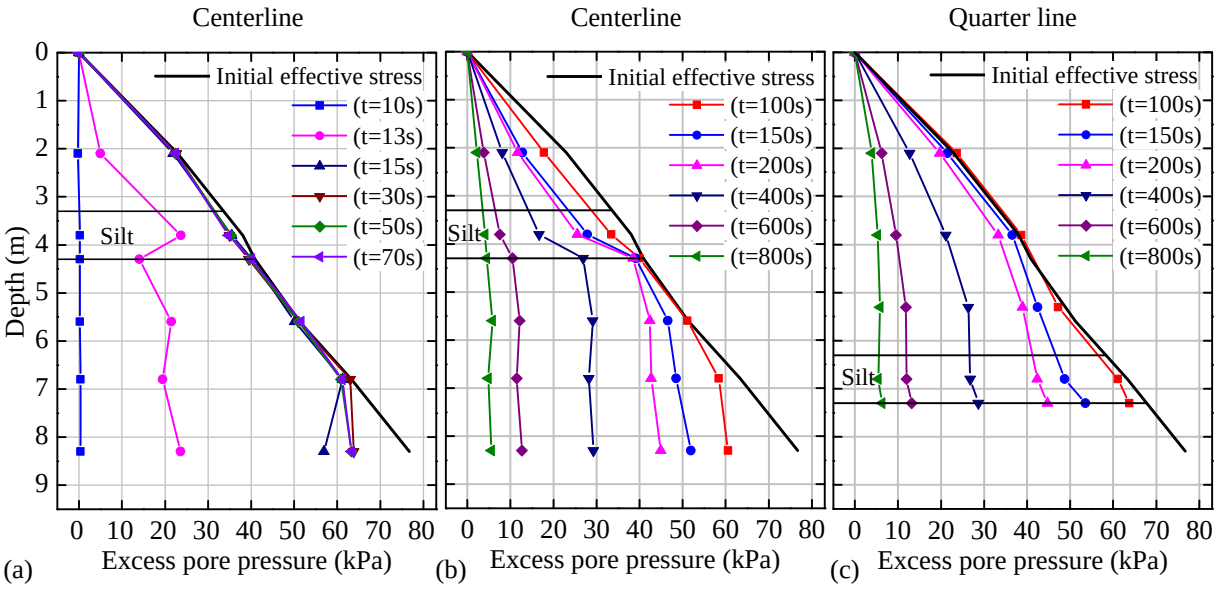

Figure 6. Excess pore water pressure isochrones in Model 3: (a) measured on centerline during shaking; (b) measured on centerline after shaking; and (c) measured on quarter line after shaking

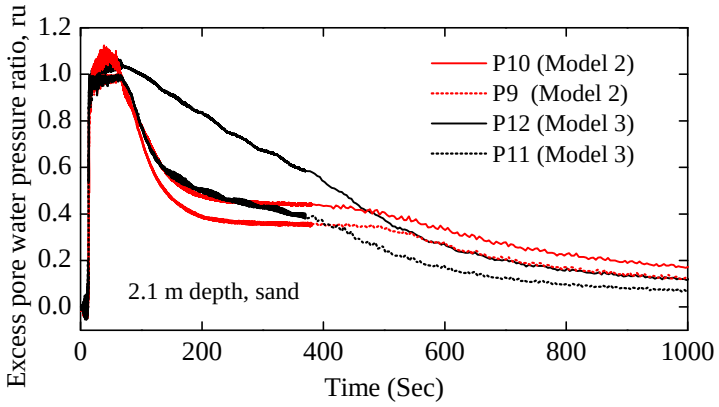

Figure 7. Excess pore water pressure ratio (r_u) at 2.1 m in Model 2 and 3

3.2. Acceleration responses

Acceleration time histories recorded during the tests are presented in Fig. 8. In Model 1, the acceleration time histories at the shallow depth, follows the imparted base motion for the first short time and attenuates for the remaining event, indicating the soil has totally liquefied (Fig. 8(a)). In Model 2 and 3, the accelerometer A1, and A3, follows the imparted input motion. However, the acceleration record above the silt layer, A5 and A9 follow imparted input motion for the first short time but damps out for the remaining event after initial liquefaction (Figs. 8(b) and 8(c)). The diminution in acceleration record at A5 for Model 2 is quite more pronounced. In this test, the bottom silt layer might be fully isolated from the bottom sand layer, as pore water is totally trapped beneath the silt layer.

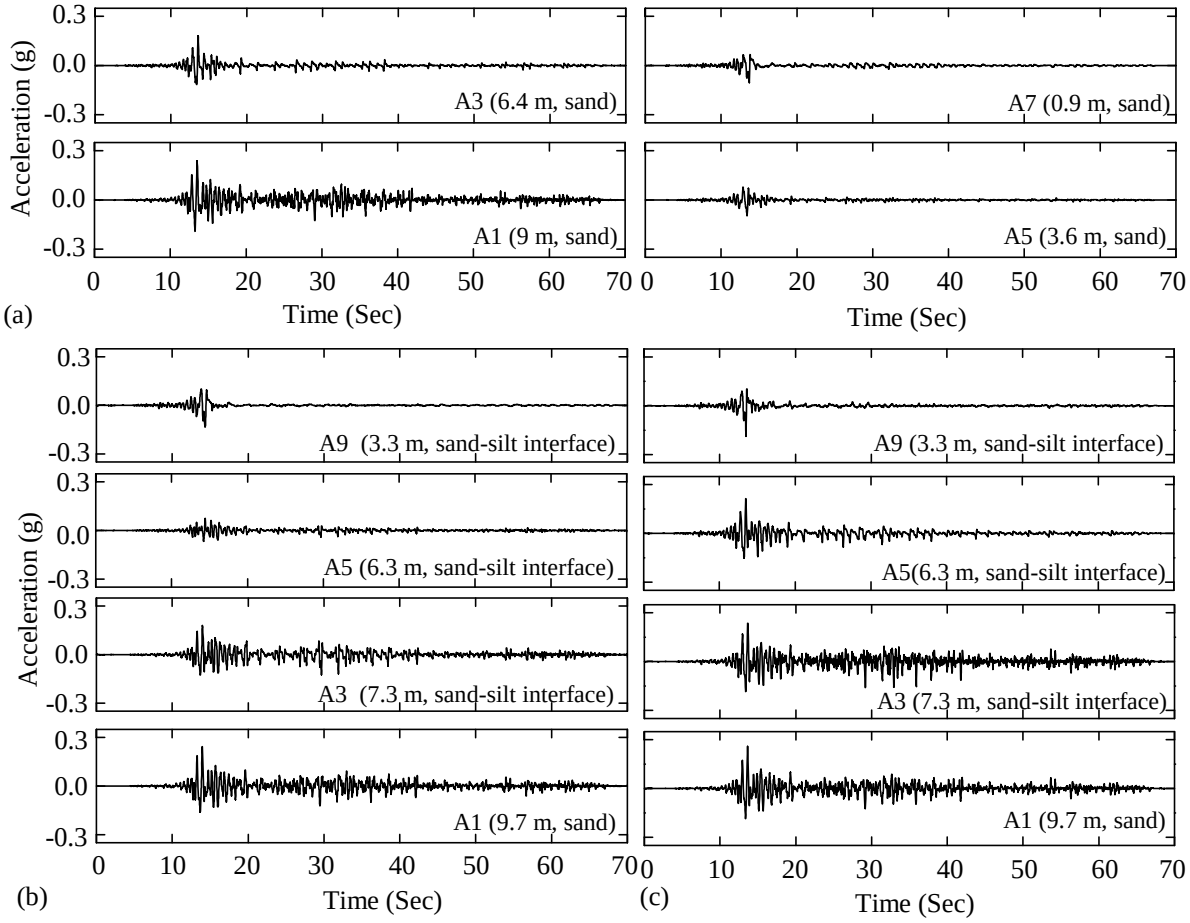

Figure 8. Acceleration time histories: (a) Model 1; (b) Model 2; and (c) Model 3

3.3. Settlement responses

Settlement time histories measured by laser displacement transducer (LDT) and potentiometers for all three tests are presented in Fig. 9. Two LDTs and two potentiometers were aligned along the centerline at the surface. An acrylic base plate was used as a target for LDTs so that they would not sink into the liquefied sand. Similarly, plexiglass was used to support the potentiometers. Potentiometers for the Model 1 malfunctioned; therefore, the records are not presented. Drastic settlements are observed during the initial process of pore water pressure build-up in all the tests. The dissipation of excess pore water pressure during seismic shaking results in soil settlement; settlement increases with increase in the amount of pore water pressure generated and drainage. Moreover, the drastic settlement during shaking might also be due to the reasons such as: penetration of target base plates into sand and compression of the dry sand etc.

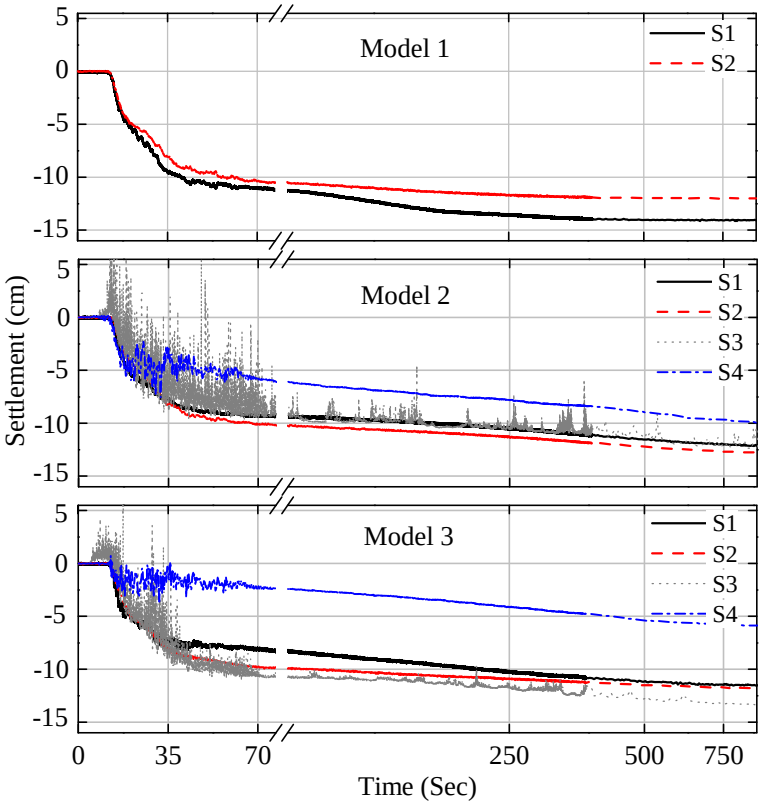

Figure 9. Settlement time histories for all the tests

Figure 10 shows the rate of settlement change after shaking at S1 for all the model tests for different time windows. It can be seen that the rate of settlement change is presumably greater in Model 1 for a certain time after shaking. However, the rate of settlement change is quite smaller after 200 s, indicating the slower dissipation of excess pore water pressure, and ceases after 400 s, indicating the total dissipation of excess pore water pressure. While the rate of settlement change for Model 3 is smaller than that for Model 1 until 160 s, the rate of settlement change for Model 3 is significantly larger than that for Model 1 after this. This reveals the rapid dissipation of excess pore water pressure within a shorter period of time due to a large value of permeability of Toyoura Sand and consequently more settlement is induced in Model 1. The continuous dissipation of excess pore water pressure in Model 3 for a longer period of time causes the rate of settlement change quite significant for a longer period of time. Moreover, the rate of settlement change for Model 3 is significantly larger for all the time windows than that for Model 2. This result shows a contrast between dissipation of excess pore water pressure and rate of settlement change (Figs. 7 and 10). The rate of settlement change for Model 2 after 200 s remains nearly constant as the excess pore pressure ratio at P10 is also nearly constant until 400 s. The dissipation is commenced after 400 s

which results in rapid settlement after this (Figs. 7 and 10). In Model 3, there is a continuous supply of pore water pressure at the discontinuous part due to seepage flow or migration of pore pressure from the surrounding soil of high pore pressure, resulting in dissipation of excess pore water pressure for a longer period of time (P12, Fig. 7) and finally causing the rate of settlement change greater at S1 in Model 3. It can be concluded that soil settlement is incorporated by the increment in the amount of pore pressure generation and drainage. The variation on amount of excess pore water pressure dissipation for the pore pressure transducers located at the same depth (P11 and P12, Fig. 7) in Model 3 causes the variation in rate of settlement change after shaking at corresponding locations. Meanwhile, the rate of settlement change is nearly the same as the amount of excess pore water pressure dissipation for the pore pressure transducers located at the same depth (P9 and P10, Fig 7) is nearly the same in Model 2. The colored noodles 'somen' placed at the sand-silt interface indicate the deformation pattern at the interface. The inspection of noodles placed during dissection also suggests that sand settled more than silt at sand-silt interface, because of larger amount of dissipation of excess pore water pressure. These results reveal that the settlement is not uniform in non-homogeneous soil deposits, causing differential settlement of the soil surface.

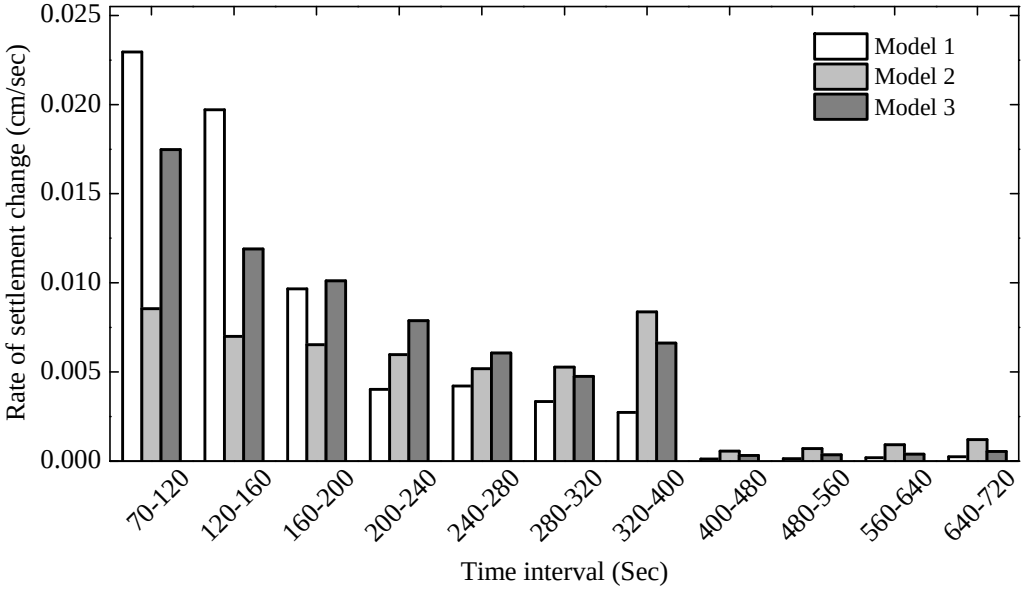

Figure 10. Variation of rate of settlement change at S1

4. CONCLUSIONS

Three centrifuge model tests were conducted to study the seismic behavior of non-homogeneous soil deposits. It was found that the pore water was trapped beneath or within less permeable soil due to the local migration of pore water and difference in permeabilities of the soils, restricting its upward movement. Continuous flow of pore water pressure was observed in the discontinuous part for a longer time period in non-homogeneous soil deposit. This might be due to the seepage flow or migration of pore pressure from the sand beneath the silt layer to the discontinuous part with relatively higher permeability. It can be concluded that the pore pressure at high pore pressure region found a path to transmit to the low pressure region, lowering the liquefaction resistance of the non-homogeneous soil. More excess pore water pressure was accumulated for a longer period of time after shaking in a non-homogeneous soil deposit than in a homogeneous soil, especially at the shallow depths. The presence of discontinuity in the less permeable soil layer can act as the drainage path, through which the excess pore water pressure can be drained out not only during but also after shaking. The rate of change of settlement at the surface, which underlies the drainage path in non-homogeneous soil deposits, was found to be significant for a longer period of time than that in the case of uniform and continuous silt layer soil deposits. It can be concluded that soil settlement is incorporated by the increment in the amount of pore pressure generation and drainage. Moreover,

test data reveals that because of non-homogeneous conditions in the soil deposits, the settlements seldom occur uniformly and thus the differential settlement may become major cause of the damage to lifelines and other facilities.

ACKNOWLEDGEMENTS

The first author is pleased to acknowledge a Monbukagakusho (Ministry of Education, Culture, Sports, Science and Technology, Japan) scholarship for graduate students. Financial support from Center for Urban Earthquake Engineering (CUEE), Tokyo Institute of Technology is gratefully acknowledged.

REFERENCES

Brennan, A. & Madabhushi, S. (2005). Liquefaction and drainage in stratified soil. *Journal of Geotechnical and Geoenvironmental Engineering,* **131,** 876-885.

Chakrabortty, P. & Popescu, R. (2012). Numerical simulation of centrifuge tests on homogeneous and heterogeneous soil models. *Computers and Geotechnics,* **41,** 95-105.

Fiegel, G. L. & Kutter, B. L. (1994). Liquefaction mechanism for layered soils. *Journal of geotechnical engineering,* **120:4,** 737-755.

Ghosh, B., Klar, A. & Madabhushi, S. P. G. (2005). Modification of Site Response in Presence of Localised Soft Layer. *Journal of Earthquake Engineering,* **9:6,** 855-876.

Kokusho, T. (1999). Water film in liquefied sand and its effect on lateral spread. *Journal of Geotechnical and Geoenvironmental Engineering,* **125:10,** 817-826.

Kokusho, T. (2000). Mechanism for water film generation and lateral flow in liquified sand layer. *Soils and Foundations,* **40:5,** 99-111.

Kokusho, T. & Kojima, T. (2002). Mechanism for postliquefaction water film generation in layered sand. *Journal of Geotechnical and Geoenvironmental Engineering,* **128:2,** 129-137.

Kramer, S. L. (1996). Geotechnical earthquake engineering, Prentice Hall.

Kulasingam, R., Malvick, E. J., Boulanger, R. W. & Kutter, B. L. (2004). Strength loss and localization at silt interlayers in slopes of liquefied sand. *Journal of Geotechnical and Geoenvironmental Engineering,* **130,** 1192-1202.

National Research Council, B. (1985). Liquefaction of soils during earthquakes, National Academy Press.

Okamura, M., Abdoun, T. H., Dobry, R., Sharp, M. K. & Taboada, V. M. (2001). Effects of sand permeability and weak aftershocks on earthquake-induced lateral spreading. *Soils and Foundations,* **41:6,** 63-77.

Stewart, D. P., Chen, Y. R. & Kutter, B. L. (1998). Experience with the use of methylcellulose as a viscous pore fluid in centrifuge models. *ASTM Geotechnical Testing Journal,* **21:4,** 365-369.

Takemura, J., Kondoh, M., Esaki, T., Kouda, M. & Kusakabe, O. (1999). Centrifuge model tests on double propped wall excavation in soft clay. *Soils and Foundations,* **39:3,** 75-87.